Micro-elastohydrodynamic lubrication of coated cylinders using coupled differential deflection method

A. A. Elsharkawy, M. J. A. Holmes, H. P. Evans and R. W. Snidle

Proceedings of the Institution of Mechanical Engineers, Part J: Journal of Engineering Tribology 2006 220: 29
DOI: 10.1243/13506501J10005

Micro-elastohydrodynamic lubrication of coated cylinders using coupled differential deflection method

A A Elsharkawy*, **M J A Holmes, H P Evans,** and **R W Snidle**
Cardiff School of Engineering, Cardiff University, Cardiff, UK

The manuscript was received on 4 March 2005 and was accepted after revision for publication on 20 January 2006.

DOI: 10.1243/13506501J10005

Abstract: A numerical solution for the micro-elastohydrodynamic lubrication (EHL) problem of two coated elastic bodies in line contact is presented. This incorporates non-Newtonian behaviour of the lubricant, using an Eyring-type non-linear viscous model. The surface elastic deformations are computed from full elasticity analysis of layered elastic half-spaces. The coupled differential deflection method is used in the numerical solution of the micro-EHL mathematical model. Results are presented for smooth surface, steady-state problems that compare the influence of coating elastic modulus and coating thickness on calculated lubricant pressure and film thickness distributions. Some transient results are also included, where the effect of coatings on a single ridge feature and on a rough surface in rolling/sliding contact is examined.

Keywords: EHL, coatings, transient EHL, rough surfaces

1 INTRODUCTION

The use of coatings to enhance the tribological performance of surfaces has grown considerably in recent years. Various coatings are now used routinely in many applications where surfaces slide and roll together under conditions of marginal lubrication, such as those occurring, for example, in devices like fuel pumps. The thickness of these coatings is generally in the range of 100 nm to 500 μm, but of particular significance are the types described as thin, hard coatings, which are typically a few microns in thickness. This class of coatings includes types such as titanium nitride (TiN), titanium carbide (TiC), aluminum oxide (Al_2O_3), and silicon carbide (SiC). Two types that have been investigated recently [**1**] as a possible means of improving the surface durability of gears are the 'super-hard' diamond-like carbon and boron carbide (B_4C) coatings. The lubrication conditions in gear tooth contacts are particularly severe because of the high contact pressures (in excess of 1 GPa) and the lack of a full fluid film because of the presence of roughness on the tooth surfaces. In these circumstances, significant asperity interactions occur, leading to transient metal-to-metal contact at asperities. Under such partial or 'mixed' lubrication conditions, there is considerable interest in using coating technology to mitigate these effects, and thin hard coatings appear to provide protection against adhesion and scuffing during these severe encounters. The analysis reported in this article is aimed at developing an understanding of the effect of coatings in lubricated contacts.

In order to understand and predict the response of thin coatings in tribological situations, it is necessary to carry out analyses of their behaviour in contact simulations under both dry and lubricated conditions. The analysis of dry, coated (layered) contacts has received considerable attention and two main techniques are used. The first approach is based on the solution of an integral equation whose kernels are determined using a Fourier transformation method [**2**–**5**]. The second technique uses the finite element (FE) method [**6**–**10**], and both elastic and elastic/plastic behaviour has been considered. The

**Corresponding author: Mechanical Engineering Department, College of Engineering and Petroleum, Kuwait University, PO Box 5969, Safat 13060, Kuwait. email: abdallah@kuc01.kuniv.edu.kw*

study of layered contacts under elastohydrodynamic lubrication (EHL) conditions is less advanced, but solutions have been obtained for the case of an elastomeric layer bonded to an elastic substrate [**11**–**14**]. These solutions show that the presence of a surface layer having elastic properties different from those of the substrate can have a significant effect on the main features of the pressure distribution and lubricant film profile.

In considering the EHL response of real engineering surfaces, it is important to include the effect of surface roughness because in most cases, the roughness is of the same order, or even larger, than the film that can be generated hydrodynamically. This is the regime occurring in most types of gears, for example, and the term micro-EHL has been used to describe the lubrication mechanism involved. Micro-EHL has been modelled with sinusoidal roughness or well-defined protuberant features [**15**–**21**] or using measured (real) roughness from gears and rollers [**22**–**26**]. All these micro-EHL studies were limited to uncoated surfaces. These solutions show considerable rippling of the pressure profile as a result of roughness, even when the nominal lubricant film is thick when compared to the amplitude of the roughness. Ripple pressures are found to be far in excess of the corresponding smooth surface (Hertzian) distribution, and this has consequences for surface fatigue (micropitting). The presence of roughness provides an opportunity for lubricant to leak from a heavily loaded rolling contact, and this mechanism provides a possible explanation for the practical problem of scuffing [**27**].

In simulations of the most severe conditions of micro-EHL, the film is found to break down, leading to direct momentary 'dry' contact between opposing asperity tips. This is the regime described as 'mixed' EHL because the surfaces are supported by a mixture of fluid pressure and dry contact.

Figure 1 illustrates the lubricated line contact between two rollers a and b. Each body is coated with perfectly bonded multiple thin elastic layers (only two layers are shown for illustration). Each layer is of uniform thickness, and a load w_z is applied to press the two bodies together. The two elastic bodies have surface velocities u_a and u_b relative to the contact point, and this motion draws lubricant into the contact so that the surfaces of the two coated bodies are completely separated by a hydrodynamic film.

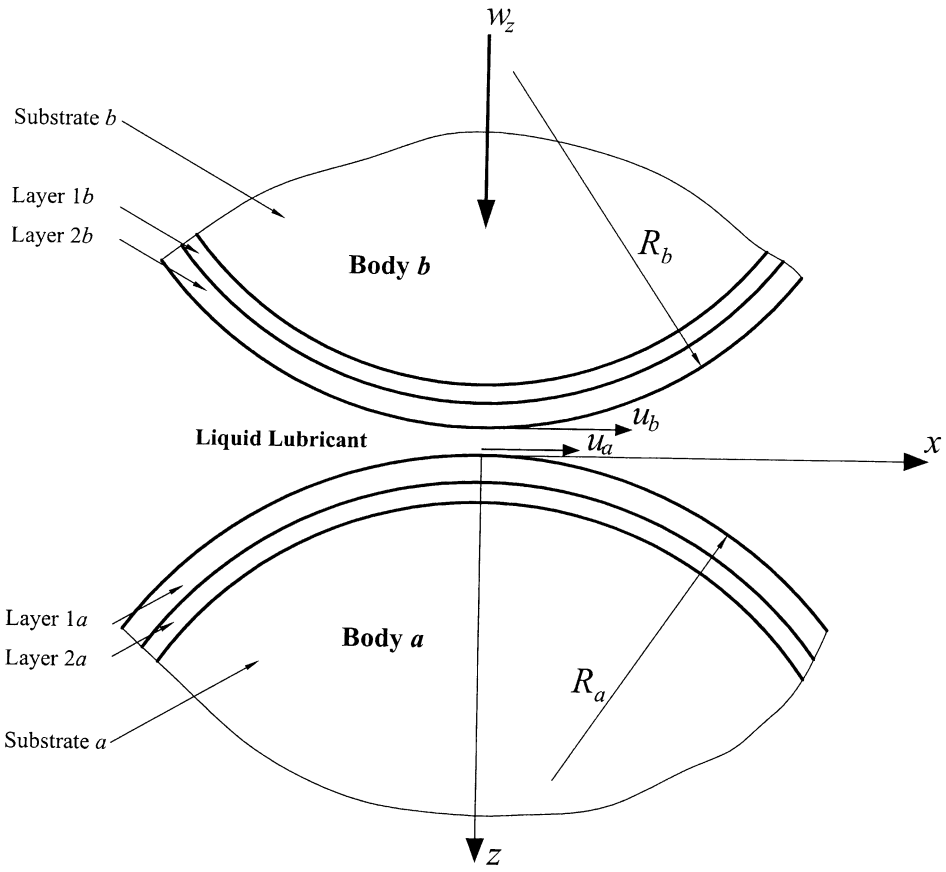

Fig. 1 Representation of two coated cylindrical bodies in a lubricated contact

The objective of the study reported in this article was to investigate the effects of surface coating (material and thickness) on the pressure and film thickness response in EHL and rough surface micro-EHL line contacts. Thermal effects within the contact are neglected at this stage, and the analysis is isothermal. A modified form of the Reynolds equation, which incorporates the non-linear viscous fluid model of Johnson and Tevaarwark [**28**] is used. The surface elastic deformations are computed from full elasticity analysis of a layered elastic half-space after Elsharkawy and Hamrock [**4**]. The dry contact problem is solved first in order to determine the corresponding 'Hertzian' half-width of contact b, the maximum contact pressure p_0, and the dry contact pressure distribution. The coupled differential deflection method developed by Hughes *et al.* [**29**] and Elcoate *et al.* [**30**] is then used to solve the EHL problem (or micro-EHL if the surface roughness is incorporated) in order to predict the hydrodynamic pressure profile and film shape. A study is presented, which investigates the effects of single layered surface coatings (with and without surface irregularities) on the pressure profile and film thickness behaviour.

2 MULTILAYERED ELASTIC HALF-SPACE

An elastic half-space coated with a number of thin elastic layers is shown in Fig. 2. These layers are assumed to be bonded together. An arbitrary normal surface pressure $p(x)$ and tangential surface traction $q(x)$ are applied on the surface. The general solution for a two-dimensional plane strain problem has been expressed in terms of Fourier integrals by Sneddon [**31**]. With reference to the coordinate system shown in Fig. 2, the stresses and the displacements are given by

$$\sigma_x = \frac{\partial^2 \phi}{\partial z^2} = \frac{1}{2\pi}\int_{-\infty}^{\infty} \frac{\mathrm{d}^2 G}{\mathrm{d}z^2} \mathrm{e}^{-i\omega x}\, \mathrm{d}\omega \tag{1}$$

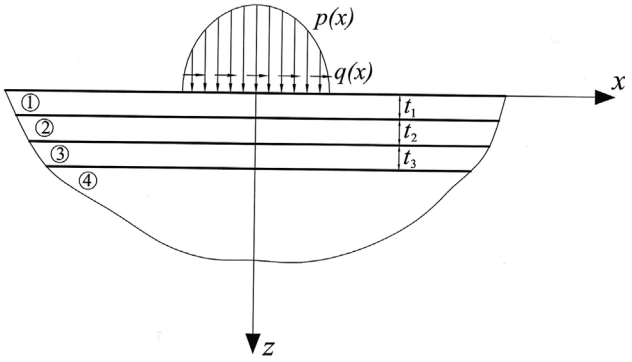

Fig. 2 Multilayered elastic half-space

$$\sigma_z = \frac{\partial^2 \phi}{\partial x^2} = -\frac{1}{2\pi}\int_{-\infty}^{\infty} \omega^2 G \mathrm{e}^{-i\omega x}\, \mathrm{d}\omega \tag{2}$$

$$\tau_{xz} = \frac{\partial^2 \phi}{\partial x \partial z} = \frac{1}{2\pi}\int_{-\infty}^{\infty} i\omega \frac{\mathrm{d}G}{\mathrm{d}z} \mathrm{e}^{-i\omega x}\, \mathrm{d}\omega \tag{3}$$

$$u_x = \frac{1-\nu^2}{2\pi E}\int_{-\infty}^{\infty} \left[\frac{\mathrm{d}^2 G}{\mathrm{d}z^2} + \left(\frac{\nu}{1-\nu}\right)\omega^2 G\right] i \mathrm{e}^{-i\omega x} \frac{\mathrm{d}\omega}{\omega} \tag{4}$$

$$u_z = \frac{1-\nu^2}{2\pi E}\int_{-\infty}^{\infty} \left[\frac{\mathrm{d}^3 G}{\mathrm{d}z^3} + \left(\frac{2-\nu}{1-\nu}\right)\omega^2 \frac{\mathrm{d}G}{\mathrm{d}z}\right] \mathrm{e}^{-i\omega x} \frac{\mathrm{d}\omega}{\omega^2} \tag{5}$$

where $G(\omega, z)$ is the Fourier transformation for the Airy stress function $\phi(\omega, z)$, E is the modulus of elasticity, ν is the Possion's ratio, and $i = \sqrt{-1}$ in equations (1) to (5) only. The general solution for G is of the form $G(\omega, z) = (A_1 + A_2 z)\mathrm{e}^{-|\omega| z_i} + (A_3 + A_4 z)\mathrm{e}^{|\omega| z_i}$ so that for the layered system illustrated in Fig. 2 the transformed function $G(\omega, z)$ can be written for any layer i as

$$G_i(\omega, z_i) = (A_{1,i} + A_{2,i}\, z_i)\mathrm{e}^{-|\omega| z_i} + (A_{3,i} + A_{4,i}\, z_i)\mathrm{e}^{|\omega| z_i} \tag{6}$$

The coefficients $A_{m,i}(\omega)$, where $m = 1, 2, 3, 4$ and $i = 1, 2, \ldots, N_\lambda$, where N_λ is the number of layers, can be determined by applying the following boundary conditions at the surface and at each interface between adjacent layers.

Outside the contact region: $(\sigma_z)_{z=0} = (\tau_{xz})_{z=0} = 0$

Inside the contact region: $(\sigma_z)_{z=0} = -p(x)$, $(\tau_{xz})_{z=0} = -q(x)$

At a large distance from the contact region, the stresses will die out so that

$$\sigma_x, \sigma_z, \tau_{xz} \to 0 \text{ as } x \to \pm\infty \text{ and } z \to \infty$$

At the interface between layer i and layer $i+1$, the stresses and displacements should be continuous because the layers are completely bonded to each other

$$(\tau_{xz})_i = (\tau_{xz})_{i+1}, \quad (\sigma_z)_i = (\sigma_z)_{i+1},$$
$$(u_z)_i = (u_z)_{i+1}, \quad (u_x)_i = (u_x)_{i+1}$$

Details of how the coefficients $A_{m,i}(\omega)$ can be determined are given in reference [**4**].

3 SURFACE ELASTIC DEFORMATION

In conventional EHL analysis, the surface elastic deformation is computed for a semi-infinite elastic solid. In order to investigate the effects of surface coating on EHL performance, the surface elastic deformation due to pressure loading may be

computed for a multilayered elastic half-space [**4**] as

$$u_z(x) = \frac{2}{\pi E'_\lambda}\int_{x_{\min}}^{x_{\text{end}}}\left\{\int_0^\infty [\beta_1 F_{\text{a}}(s) + \beta_2 F_{\text{b}}(s)] \times \cos\left[s\left(\frac{x-x'}{t_{\text{T}}}\right)\right]\text{d}s\right\} p(x')\text{d}x' \tag{7}$$

(Note that in reference [**4**], the expressions given are for relative rather than absolute deflections.) In equation (7)

$$F_{\text{a}}(s) = \left(\frac{\text{d}^3 G_{1\text{a}}}{\text{d}\zeta^3} - \frac{2-\nu_{1\text{a}}}{1-\nu_{1\text{a}}}s^2\frac{\text{d}G_{1\text{a}}}{\text{d}\zeta}\right)_{\zeta=0}\frac{1}{s^2} \tag{8}$$

$$F_{\text{b}}(s) = \left(\frac{\text{d}^3 G_{1\text{b}}}{\text{d}\zeta^3} - \frac{2-\nu_{1\text{b}}}{1-\nu_{1\text{b}}}s^2\frac{\text{d}G_{1\text{b}}}{\text{d}\zeta}\right)_{\zeta=0}\frac{1}{s^2} \tag{9}$$

$$t_{\text{T}} = \sum_{i=1}^{N_\lambda} t_i \tag{10}$$

$$\beta_1 = \frac{(1-\nu_{1\text{a}}^2)E_{1\text{b}}}{(1-\nu_{1\text{b}}^2)E_{1\text{a}} + (1-\nu_{1\text{a}}^2)E_{1\text{b}}} \tag{11}$$

$$\beta_2 = \frac{(1-\nu_{1\text{b}}^2)E_{1\text{a}}}{(1-\nu_{1\text{b}}^2)E_{1\text{a}} + (1-\nu_{1\text{a}}^2)E_{1\text{b}}} \tag{12}$$

$$E'_\lambda = \frac{2E_{1\text{a}}E_{1\text{b}}}{(1-\nu_{1\text{b}}^2)E_{1\text{a}} + (1-\nu_{1\text{a}}^2)E_{1\text{b}}} \tag{13}$$

In these equations $s = \omega t_{\text{T}}$, $\zeta = z/t_{\text{T}}$, t_{T} is total thickness of layers, $x_{\min}$ and x_{end} are the two boundary points of the conjunction beyond which the pressure vanishes, and subscripts a and b are used to denote body a and body b, respectively (Fig. 1).

For large values of s, both $F_{\text{a}}(s)$ and $F_{\text{b}}(s)$ will tend to $2/s$. Therefore, the integral from 0 to ∞ can be divided into two regions, one from 0 to s_0 where $F_{\text{a}}(s)$ and $F_{\text{b}}(s)$ are given by equations (8) and (9), and another from s_0 to ∞, where the approximation $2/s$ is used for these terms. The first integration is computed numerically by using a semi-open integration formula because the integrand is singular at $s = 0$. A closed form solution for the second integral can be obtained, and values of $s_0 > 3$ are usually sufficient to ensure that the approximation involved in $F_{\text{a}}(s)$ and $F_{\text{b}}(s)$ does not affect the result. It is worth noting that if the two cylinders are coated with a single coating of the same material, then $\beta_1 = \beta_2 = 0.5$ and $F_{\text{a}}(s) = F_{\text{b}}(s)$.

The surface elastic deformation equation (7) can be solved numerically by dividing the lubricated region $x_{\min} \leqslant x \leqslant x_{\text{end}}$ into subintervals between mesh points x_j. By considering a linear pressure distribution in each subinterval $x_j \leqslant x' \leqslant x_{\text{j+1}}$

$$p(x') = \frac{(x'-x_{j+1})}{(x_j-x_{j+1})}p_j + \frac{(x'-x_j)}{(x_{j+1}-x_j)}p_{j+1} \tag{14}$$

The surface elastic deformation can be obtained in the following form

$$u_z(x_j) = \sum_{\text{all } k} g_{k-j}p_k \tag{15}$$

where g_{k-j} is the influence coefficient at point j due to a unit load at point k. In order to use the coupled differential deflection method developed by Hughes *et al.* [**29**], the surface elastic deformation is formulated in a differential form as

$$\frac{\partial^2 u_z(x_j)}{\text{d}x^2} = \frac{u_z(x_{j+1}) - 2u_z(x_j) + u_z(x_{j-1})}{\Delta x^2} = \sum_{\text{all } k} f_{k-j}\, p_k \tag{16}$$

The coefficients f_k decay rapidly as $|k|$ increases from zero in comparison with coefficients g_k. This sharp decay ensures that the effect of pressure on the second derivative of deflection is highly localized and leads directly to the major advantage of this technique, which is the ability to fully couple the discretized elastic and hydrodynamic equations within a highly banded matrix structure.

For uncoated bodies the influence coefficients f_k are formally derived by differentiation of the deflection equation [**32**]. In the case of coated surfaces, the complexity of equation (7) and its associated terms mean that this route to obtaining the coefficients is extremely involved, and the simpler approach of differencing the g_k coefficients as implicit in equation (16), is used. Thus, the f_k coefficients are obtained directly from the g_k coefficients by

$$f_k = \frac{g_{k-1} - 2\,g_k + g_{k+1}}{\Delta x^2} \tag{17}$$

It may be emphasized that this differential treatment of the elastic deflection calculation, that is, replacing equation (15) with equation (16), gives rise to essentially identical calculated deflection for the same pressure distributions [**32**]. Comparisons of EHL solutions produced using the two formulations show the calculated film thickness for rough surface problems to differ by less than 0.4 per cent of the local film thickness value [**29**]. For the current approach using equation (17), the results of such a comparison can be expected to be identical because equation (16) is a linear combination of equation (15) at three neighbouring mesh points.

4 DRY CONTACT ANALYSIS

The frictionless dry line contact problem between two multilayered elastic rollers can be formulated as follows [**4**]

$$\frac{2}{\pi E'_\lambda}\int_{-b}^{b}\left\{\int_0^\infty [\beta_1 F_a(s)+\beta_2 F_b(s)] \times \cos\left[s\left(\frac{x-x'}{t_T}\right)\right]\mathrm{d}s\right\}p(x')\mathrm{d}x' = \delta_0 - \frac{x^2}{2R} \tag{18}$$

$$\int_{-b}^{b} p(x')\mathrm{d}x' = w_z \tag{19}$$

where δ_0 is the deflection at the geometric centre of the contact. Equation (19) represents the equilibrium condition. An iterative numerical technique for solving the dry contact problem is implemented to determine the actual half-width of contact b and the dry contact pressure distribution $p(x)$ for given values of R, w_z, and E'_λ.

5 MICRO-EHL ANALYSIS

Under severe conditions occurring in an EHL conjunction, most lubricants exhibit non-Newtonian behaviour. Several models have been proposed to describe this non-linear response, among which is the Eyring-type model introduced by Johnson and Tevaarwerk [**28**] for predicting traction, and extensively used since for this purpose [**33**]. This model has also been widely used in numerical simulations dealing with the effect of non-Newtonian behaviour on the film thickness and pressure profile in the case of both smooth and rough surfaces [**34**–**38**].

Following Conry *et al.* [**35**], and Tao *et al.* [**38**], the mathematical formulation of the transient micro-EHL problem can be written

$$\frac{\partial(\rho h)}{\partial t} + \frac{(u_a+u_b)}{2}\frac{\partial(\rho h)}{\partial x} - \frac{\partial}{\partial x}\left(\frac{\rho h^3}{12\eta}S\frac{\partial p}{\partial x}\right) = 0 \tag{20}$$

$$\frac{\partial^2 h(x_j)}{\partial x^2} = \sum_{\text{all } k} f_{k-j}\, p_k + \frac{1}{R} + \frac{\partial^2 \phi}{\partial x^2} \tag{21}$$

$$S = \frac{3(\Sigma\cosh\Sigma - \sinh\Sigma)}{\Sigma^3} \times \sqrt{1+\frac{\eta^2(u_b-u_a)}{\tau_0^2 h^2}\frac{\Sigma^2}{\sinh^2\Sigma}} \tag{22}$$

$$\Sigma = \frac{h}{2\tau_0}\frac{dp}{dx} \tag{23}$$

$$\eta(x) = \eta_0 \exp\left\{\ln\left(\frac{\eta_0}{\kappa}\right)\left[\left(1+\chi\, p(x)\right)^{\hat{Z}} - 1\right]\right\} \tag{24}$$

$$\rho(x) = \rho_0\left[\frac{1+\gamma p(x)}{1+\lambda p(x)}\right] \tag{25}$$

$$\int_{x_{\min}}^{x_{\text{end}}} p(x)\,\mathrm{d}x = w_z \tag{26}$$

$$p = 0 \quad \text{at } x = x_{\min}$$

$$p = \frac{\partial p}{\partial x} = 0 \quad \text{at } x = x_{\text{end}} \tag{27}$$

Equation (20) is the modified Reynolds equation incorporating the Eyring-type non-linear viscous fluid model. The non-Newtonian factor S given by equation (22) depends on the pressure, film thickness, sliding speed, and pressure gradient. The dependence of both the lubricant viscosity and density on pressure is given by equations (24) and (25), respectively. Parameter $\hat{Z}$ in equation (24) is determined from the pressure coefficient of viscosity α. Equation (26) represents the load equilibrium condition. The boundary conditions given in equation (27) must also be satisfied. The surface elastic deflection process is modelled using equation (21), which requires two boundary values to be specified. The value of $h(x_{\min})$ at the entry boundary is an arbitrary constant used to obtain the required load, and equation (7) in the form of equation (15) is used to provide the second exit boundary condition by evaluation of the difference in deflection $u_z(x_{\max}) - u_z(x_{\min})$. The coupled differential deflection method, which was presented in detail by Hughes *et al.* [**29**] and Elcoate *et al.* [**30**], is utilized to solve the transient micro-EHL system described by equations (20) to (27). In this method, equations (20) and (21) are solved simultaneously with equations (22) to (27). In the current work, equation (20) is discretized using first-order FEs and equation (21) by a central difference scheme. The two equations are expressed in an overall matrix problem whose unknowns are the values of $h(x)$ and $p(x)$ at each node of the computing mesh. The rapid decay of the influence coefficients, f_k, allows the problem to be expressed in a narrow banded form [**30**].

Table 1 Operating conditions and lubricant properties

Radius of surfaces, $R_a = R_b$	0.0381 m
Elastic modulus, $E_a = E_b$	200 GPa
Poisson's ratio, $\nu_a = \nu_b$	0.3
Poisson's ratio of the coating material, ν_c	0.3
Hertzian pressure of uncoated case, p_H	0.9833 GPa
Hertzian half-width of uncoated case, b_H	0.3409×10^{-3}m
Surface velocity of body a, u_a	28.125 m/s
Surface velocity of body b, u_b	21.875 m/s
Viscosity of the lubricant at atmospheric pressure, η_0	0.0048 Pa s
Pressure–viscosity coefficient, α	11.1 GPa^{-1}
Pressure–viscosity index, $\hat{Z}$	0.5025
Eyring stress, τ_0	10 MPa
Parameter in equation (24), χ	5.1 GPa^{-1}
Parameter in equation (25), γ	2.266 GPa^{-1}
Parameter in equation (24), κ	63.15×10^{-6} Pa s
Parameter in equation (25), λ	1.683 GPa^{-1}

6 NUMERICAL SOLUTION

The numerical solution of the problem begins with a solution to the dry contact coated problem for the specified variables defining geometry and elastic properties of contacting bodies (R_a, R_b, E_a, E_b, ν_a, and ν_b); coating layer (t_c, E_c, and ν_c); lubricant properties (η_0, α, and τ_0); applied normal load w_z, surface velocities (u_a and u_b); surface roughness type and characteristics. This determines the corresponding half-width of contact b, the maximum dry contact pressure p_0, and the dry contact pressure distribution. The EHL or micro-EHL problem is then solved using the coupled differential deflection method [**29**, **30**]. The pressure and surface shear stress results are obtained for every timestep in the case of a transient analysis.

7 RESULTS

The operating conditions and lubricant parameters are presented in Table 1. The lubricant modelled is Mobil Jet 2, a synthetic gas turbine lubricant. The coating material and its thickness are the parameters of most interest in this investigation, and their effects on the pressure and film thickness distributions are presented. Although the analysis presented is valid for multiple layers, the case considered is that of two bodies each coated with a single layer having the same properties (i.e. $E_{1a} = E_{1b} = E_c$, $\nu_{1a} = \nu_{1b} = \nu_c$, and $t_{1a} = t_{1b} = t_c$). The ranges of elastic modulus and layer thickness considered are $10\,\text{GPa} \leqslant Ec \leqslant 400\,\text{GPa}$ and $1\,\mu\text{m} \leqslant t_c \leqslant 100\,\mu\text{m}$, respectively. The elastic modulus for steel (200 GPa) is considered as a reference so that coatings with $E > 200$ GPa are considered 'hard' and those with $E < 200$ GPa are considered 'soft' (the words hard and soft are used somewhat loosely in this way and do not describe the hardness of the coatings in the sense of the flow pressure, which is not a consideration in the current study).

The computational domain in the EHL analysis is taken as $-3b \leqslant x \leqslant 2b$ with uniform mesh discretization of $\Delta x = b/100$ in the case of smooth surfaces and $\Delta x = b/200$ in the case of rough surfaces. The computer code was first validated for both dry and lubricated contacts. If the coating material is the same as the substrate, the problem becomes the conventional (uncoated) EHL problem because the coating layer is assumed to adhere completely to the cylinder it covers. Therefore, for any coating thickness, the results should be in agreement with the uncoated EHL problems. Figure 3 shows a comparison of the rate of decay of the normalized weighting factors f_i/f_0 (solid lines), and g_i/g_0 (dashed lines) obtained from multilayered analysis when $E_c = 200$ GPa and $t_c = 1\,\mu$m. The normalized coefficients f_i/f_0 can be seen to decay significantly faster than the g_i/g_0 coefficients. The advantage of rapid decay of f_i/f_0 is not, therefore, compromised by the inclusion of coatings in the analysis. Figure 3 also includes the corresponding coefficient variations for the uncoated problem, which are obtained analytically. The differences can be seen to be small and are attributable to the evaluation of g_k by numerical integration in the case of the thin coatings (1 μm) adopted. For thicker coatings, the difference in coefficients diminishes. The differences shown in Fig. 3 have no effect in determining the EHL solution. This can be seen in Fig. 4 which shows the pressure

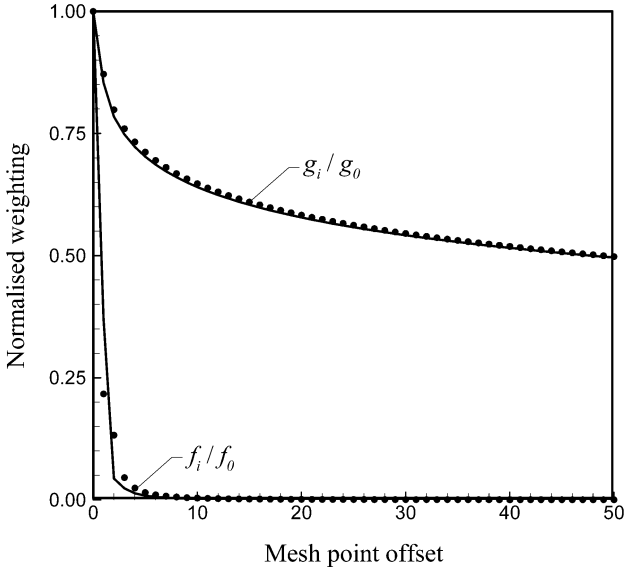

Fig. 3 Comparison between normalized weighting factors g_i/g_0 and f_i/f_0 obtained from multilayered analysis when $E_c = 200$GPa and $t_c = 1\mu$m (symbols) and those obtained from uncoated analysis (solid lines)

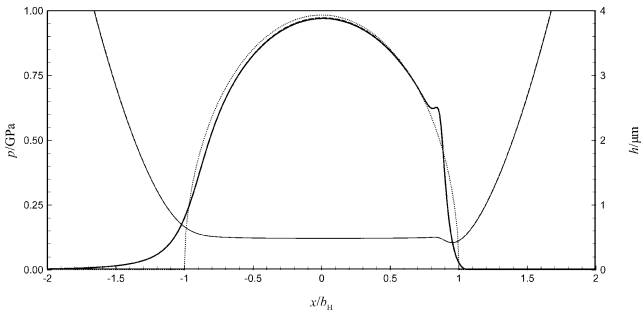

Fig. 4 Comparison of pressure profile and film shape when f_i and g_i are obtained from multilayered analysis when $E_c = 200$ GPa and $t_c = 1\mu$m (solid lines), dry contact pressure (dotted), with those obtained from uncoated analysis (dashed lines)

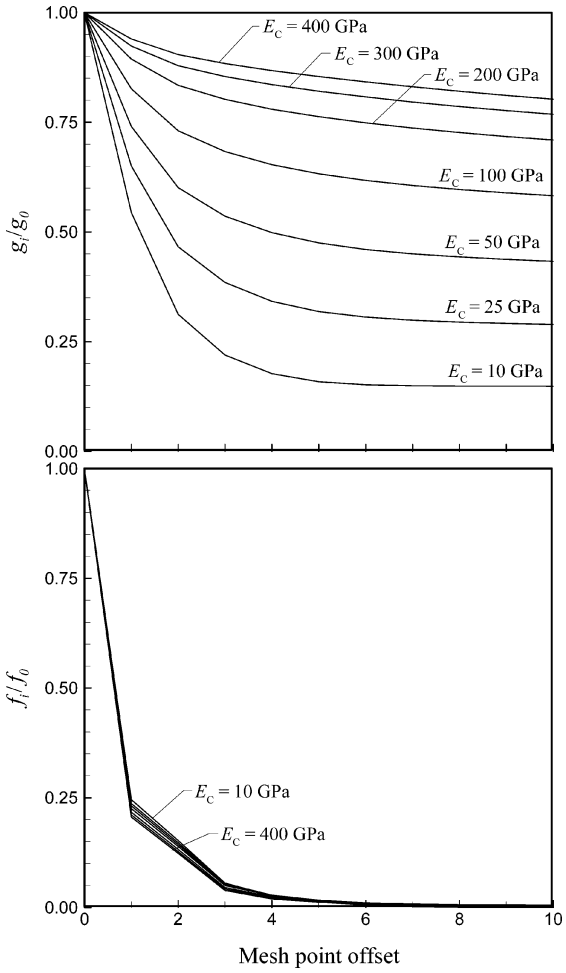

Fig. 5 Normalized weighting factors g_i/g_0, and f_i/f_0 for various values of the elastic modulus of the coating material E_c when $t_c = 20$ μm

distribution and film thickness obtained for this case and also includes the corresponding curves obtained from solving the equivalent uncoated problem. The results presented are indistinguishable.

Figure 5 shows the effect of the elastic modulus of the coating material E_c on the normalized weighting factors g_i/g_0 and f_i/f_0 in the case of smooth surface. The coating thickness t_c was fixed at 20 μm. The value of E_c can be seen to have a significant effect of E_c on the rate of decay of g_i/g_0, whereas its effect on the decay of f_i/f_0 is much smaller. The pressure and film thickness distributions for a series of values of E_c for the case of a smooth surface contact are shown in Fig. 6. The results are presented in terms of the contact dimension, b_H, for the uncoated case. It is to be expected that surface elastic deformations will increase when the elastic modulus of the coating material is reduced. Reducing E_c causes an increase in the contact area, with a consequent reduction in the maximum pressure. The pressure spike in the exit part of the contact is decreased as the coating stiffness is reduced and has disappeared for coatings with $E_c < 50$ GPa. In contrast, the pressure spike is exacerbated in the case of coatings with $E_c > 200$ GPa because of the increase in the viscosity caused by the resulting high pressure. It is interesting to note that, in spite of the changes in contact area, the difference in film thickness between the various coating modulus values is very small.

Figure 7 shows the effect of the coating thickness t_c on the pressure and film thickness profiles in the case of a smooth surface. For this comparison, the elastic modulus of the coating material was fixed at

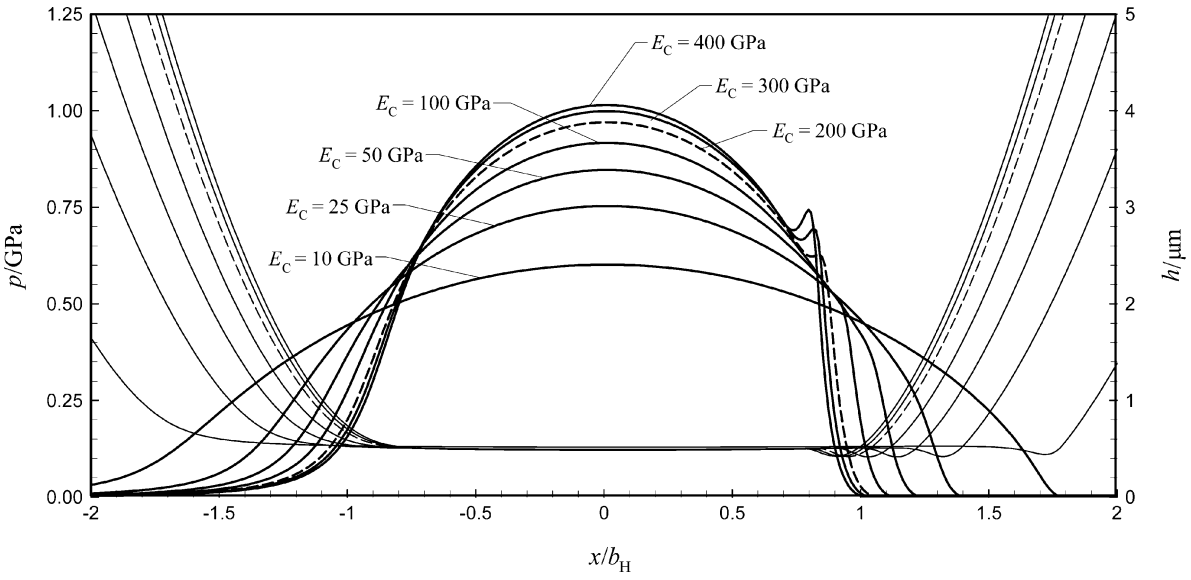

Fig. 6 Pressure distributions and film shapes for various values of the elastic modulus of the coating material E_c when $t_c = 20$ μm

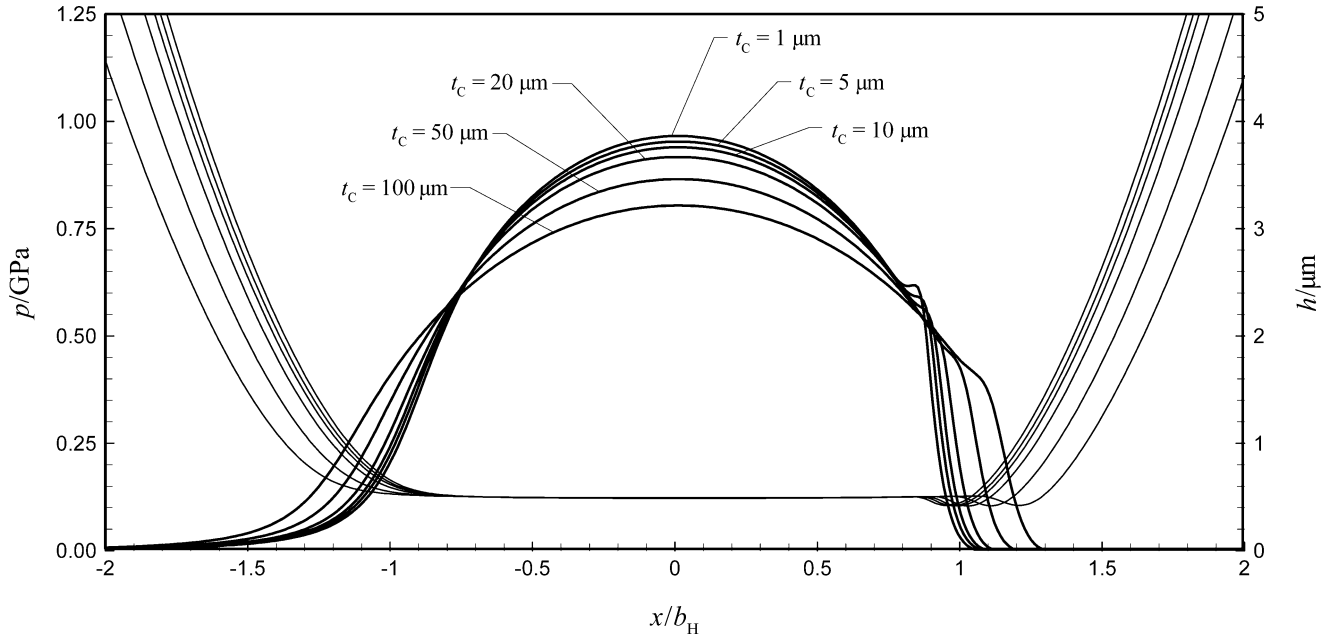

Fig. 7 Pressure distributions and film shapes for various values of the coating thickness t_c when $E_c = 100$ GPa(soft coating)

100 GPa (soft coating). The results show that as the coating thickness increases, the width of the contact area increases, with a consequent reduction in the magnitude of pressure. This is because the elastic deformations in the case of a soft coating increase as the coating thickness increases. Figure 8 makes the corresponding comparison for the case of $E_c = 400$ GPa (hard coating). Here, it can be seen that the coating thickness has an inverse effect on the pressure and the width of the lubricated region in comparison with the soft coating case of Fig. 7, i.e. a reduction in contact area and an increase in pressure as the coating thickness is increased. The effect of the coating thickness on the film shape

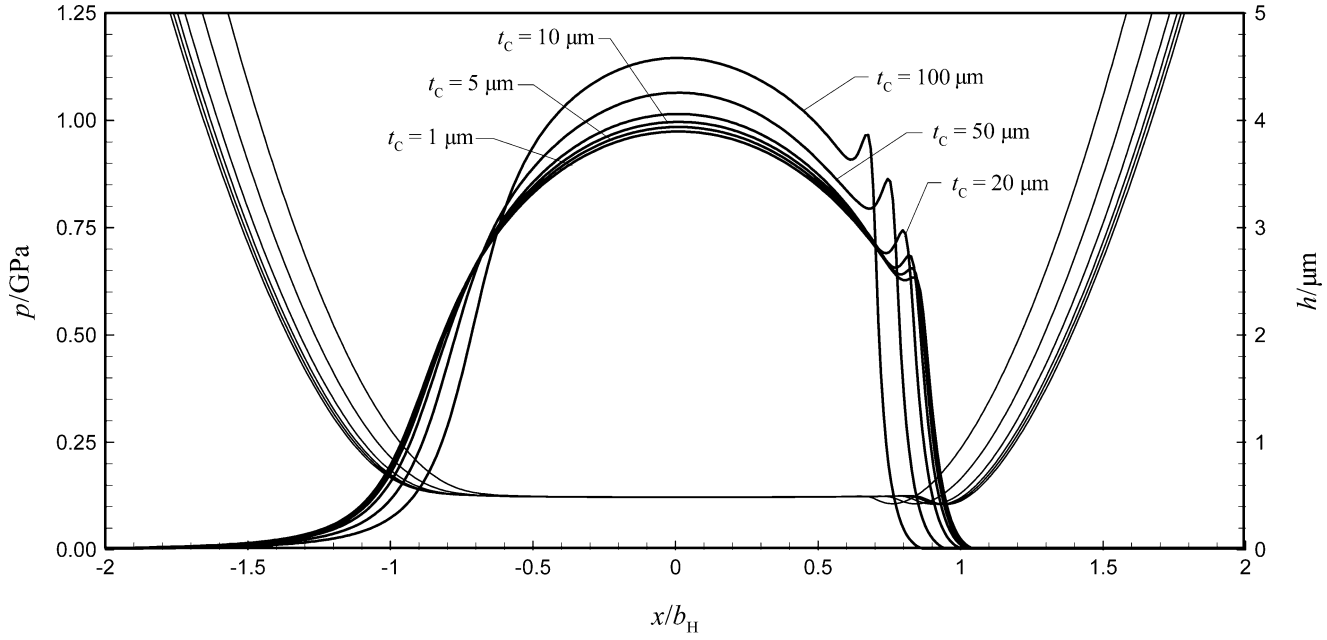

Fig. 8 Pressure distributions and film shapes for various values of the coating thickness t_c when $E_c = 400$ GPa (hard coating)

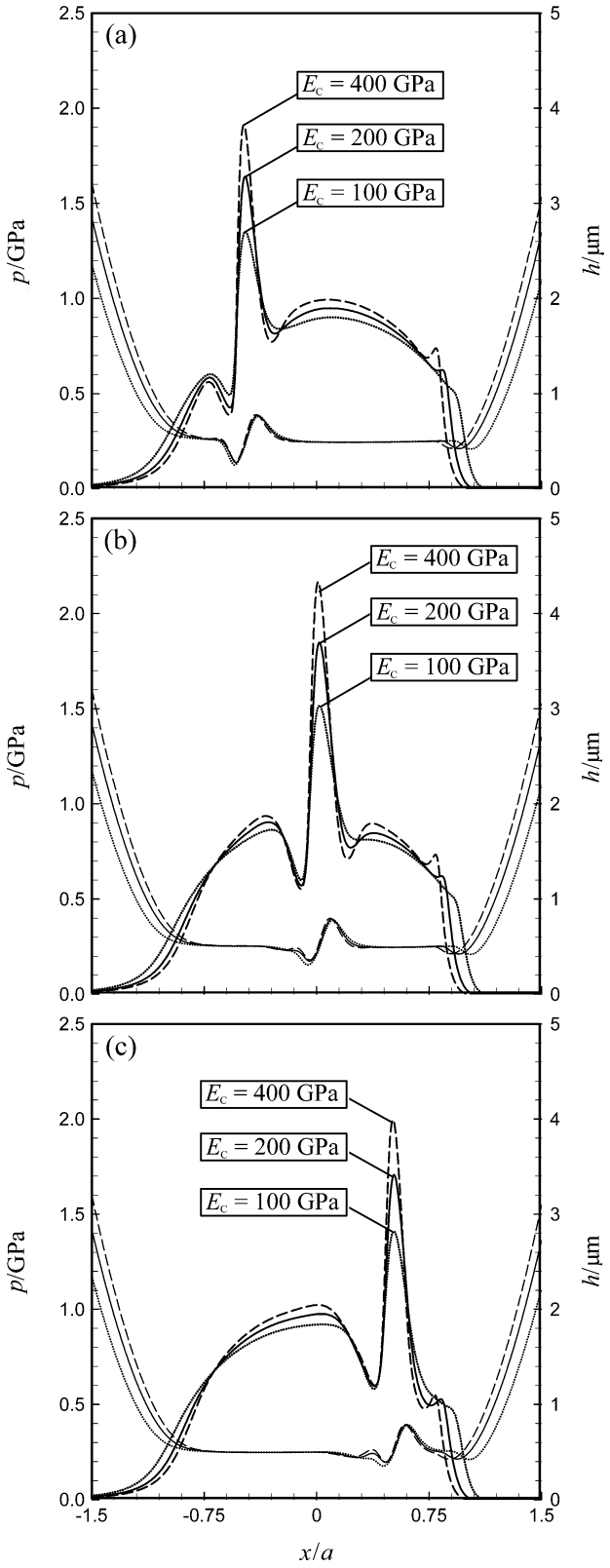

Fig. 9 Effect of a moving ridge on transient pressure distribution and film shapes for various values of the elastic modulus of the coating material E_c when $t_c = 20\,\mu m$. (a) $x_b/b_H = -0.5$, (b) $x_b/b_H = 0$, and (c) $x_b/b_H = 0.5$

within the contact region is not significant, as can be seen from Figs 7 and 8.

Figure 9 shows the effect of a moving ridge on the transient pressure distribution and film shapes for three different values of the elastic modulus of the coating material E_c. The ridge assumed is the modulated cosine form introduced by Venner and Lubrecht [**39**], which has the formula

$$\phi = A_b \times 10^{-10[(x-x_b)/W_b]} \cos\left(2\pi \frac{x - x_b}{W_b}\right) \tag{28}$$

Here, A_b represents constant amplitude, W_b is the waviness length, and x_b is the position of the centre of the ridge. The parameters chosen are $A_b = 0.5\,\mu m$ and $W_b = 170\,\mu m$ and the ridge is part of the faster moving surface. The pressure distributions and film shapes are displayed at three positions of the ridge during its transit of the contact area, $x_b/b_H = -0.5, 0, 0.5$. A coating thickness of 20 μm was used with three coating modulus values, 100, 200, and 400 GPa. It can be seen that the maximum pressure developed because of the effect of the ridge is reduced by 18 per cent in the case of the soft coating ($E_c = 100$ GPa) and increased by 17 per cent in the case of the hard coating ($E_c = 400$ GPa) compared with the uncoated case ($E_c = 200$ GPa).

Figure 10 illustrates the roughness profile used for the results presented in Fig. 11. This profile was taken from an FZG micropitting test carried out at QinetiQ that had been run for several load stages. The profile has a roughness average $R_a = 0.31\,\mu m$, and the rounded nature of the prominent asperities brought about by the running-in process leads to a skewed distribution of surface heights. The question of adequate mesh resolution for transient EHL analyses of rough surfaces has been considered in reference [**40**] where it is shown that for non-layered analyses with both surfaces having a roughness profile of the form of Fig. 10, the results for a mesh with

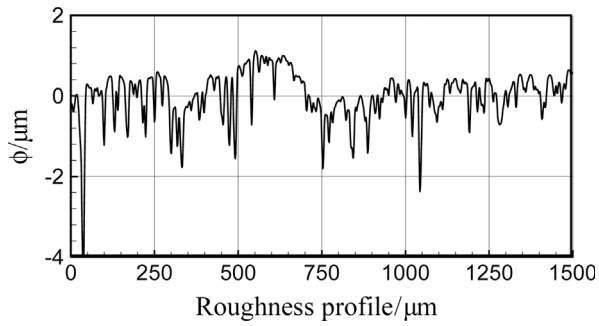

Fig. 10 Roughness profile used for the coating analysis illustrated in Fig. 11, $R_a = 0.31\,\mu m$. The profile is illustrated with the metal below the profile trace

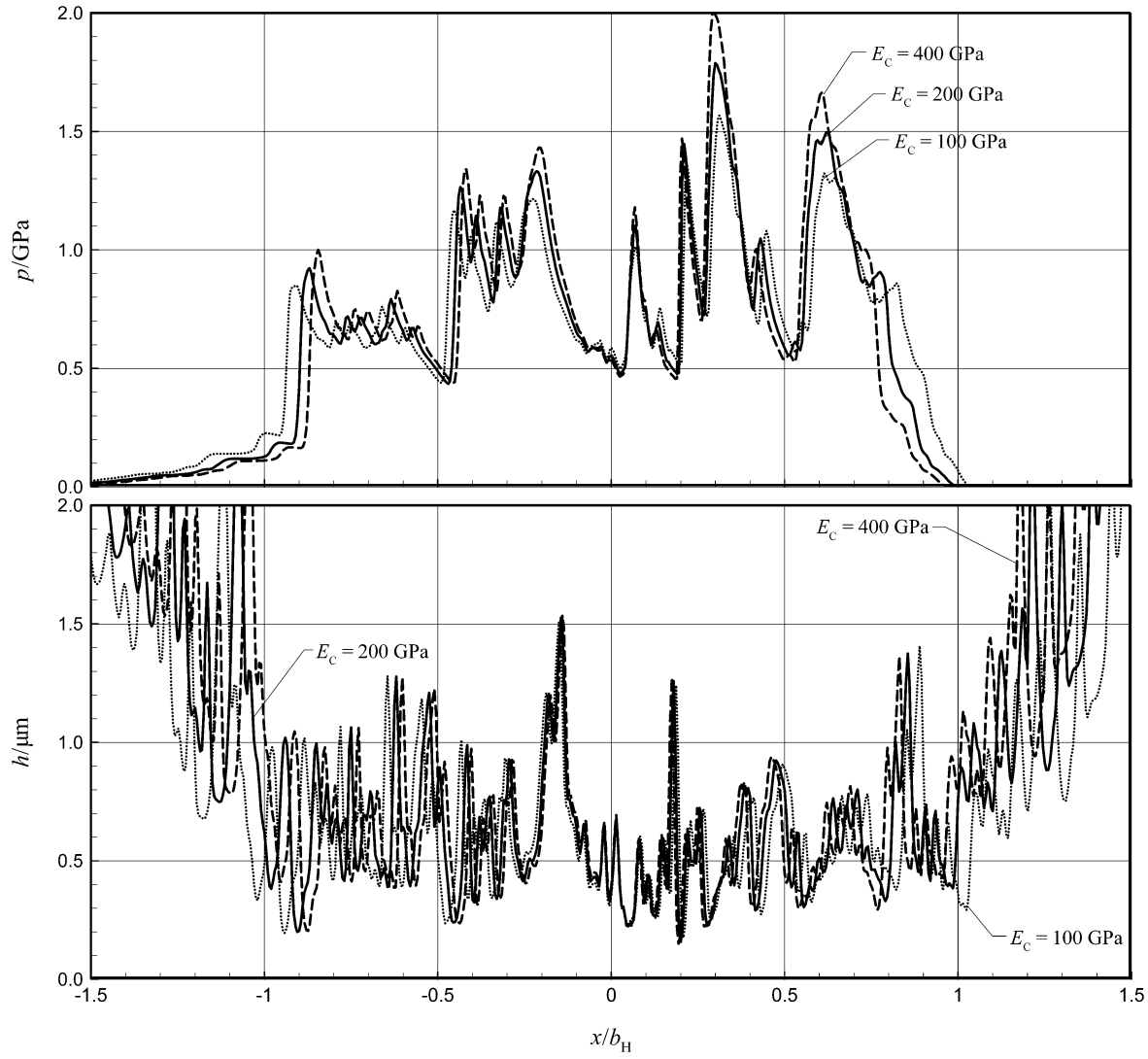

Fig. 11 Transient pressure distributions and film shapes obtained at a timestep for a single rough surface with various values of the elastic modulus of the coating material E_c when $t_c = 20\,\mu m$

$\Delta x = b/200$ are essentially the same as those for the finer mesh of $\Delta x = b/400$.

Figure 11 shows the transient pressure distributions and film shapes obtained at one particular timestep in the transient analysis of a single rough surface with three different values of the elastic modulus of the coating material E_c, and in each case, a coating thickness of $t_c = 20\ \mu m$ was specified. The soft coating reduces the asperity pressures when compared with the uncoated case. As was seen with the single roughness feature of Fig. 9, the effect of the lower modulus coating is to relieve the high pressure developed on asperity features, whereas the higher modulus coating increases the extreme pressure values. This is also seen in the transient analysis. For the asperity feature located at $x = 0.3b_H$, for example, the $E_c = 100$ GPa coating reduces the pressure by 12 per cent and the $E_c = 400$ GPa coating increases the value by 13 per cent when compared with the reference, uncoated case. This result may suggest the mechanism by which the soft coating can protect the surface from rolling contact fatigue as shown experimentally by Yoshida and Fujii [**41**].

It is worth noting that thermal effects were neglected in this study and the analysis was limited to line contacts. The surface properties of coating material may have low or high thermal conductivity in comparison with the substrate. A low conductivity coating may substantially increase the surface temperature. This temperature change will directly affect the film thickness and coefficient of friction.

8 CONCLUSIONS

An EHL analysis for coated surfaces and a transient micro-EHL analysis for two elastic bodies coated with thin elastic layers has been introduced. The differential deflection approach was adopted, and the Reynolds equation used incorporated a non-linear viscous fluid model of the Eyring-type. The surface elastic deformations are computed from full elasticity analysis of a layered elastic half-space.

The effects of surface coating modulus and thickness on the pressure and film thickness profiles obtained for smooth surfaces are presented and discussed. The steady-state smooth surface results presented suggest that as the elastic modulus of the coating material decreases, the width of the lubricated conjunction increases and the pressure and the pressure spike decrease. For low modulus coatings, as the coating thickness increases, the width of the lubricated region increases and the pressure decreases. The inverse is the case for high modulus coatings.

Results for transient cases are presented both for a single surface ridge feature and for a rough surface profile taken from a gear test experiment. These illustrate the way in which a lower modulus coating can reduce the extreme pressure values occurring at asperity features and in which a high modulus coating can cause increased extreme pressures.

ACKNOWLEDGEMENTS

Professor Elsharkawy would like to thank Kuwait University for supporting a sabbatical period at Cardiff University, which allowed this work to be carried out. The first phase of this study was supported by Research Administration Unit of Kuwait University under grant no. EM 01/02.

REFERENCES

1 **Alanou, M. P., Evans, H. P.,** and **Snidle, R. W.** Effect of different surface treatments and coatings on the scuffing performance of hardened steel disks at very high sliding speeds. *Tribol. Int.*, 2004, **37**, 93–102.

2 **Gupta, P. K.,** and **Walowit, J. A.** Contact stresses between an elastic cylinder and a layered elastic solid. *ASME J. Lubr. Technol.*, 1974, **96**, 250–257.

3 **King, R. B.** and **O'Sullivan, T. C.** Sliding stresses in a two-dimensional layered elastic half-space. *Int. J. Solids Struct.*, 1987, **23**(5), 581–597.

4 **Elsharkawy, A. A.** and **Hamrock, B. J.** A numerical solution for dry sliding line contact of multilayered elastic solids. *Trans ASME J. Tribol.*, 1993, **115**(2), 237–245.

5 **Mao, K., Bell, T.,** and **Sun, Y.** Effect of sliding friction on contact stresses for multilayered elastic bodies with rough surfaces. *Trans ASME J. Tribol.*, 1997, **119**, 476–480.

6 **Ihara, T., Shaw, M. G.,** and **Bhushan, B. A.** Finite element analysis of contact stress and strain in an elastic film on a rigid substrate–part I: zero friction. *Trans ASME J. Tribol.*, 1986, **108**(4), 527–533.

7 **Komvopoulos, K.** Finite element analysis of a layered elastic solid in normal contact with a rigid substrate. *Trans ASME J. Tribol.*, 1988, **110**(3), 477–597.

8 **Tian, H.** and **Saka, N.** Finite element analysis of an elastic–plastic two-layer half space: sliding contact. *Wear*, 1991, **148**, 262–285.

9 **Anderson, I. A.** and **Collins, I. F.** Plane strain stress distributions in discrete and blended coated solids under normal and sliding contact. *Wear*, 1995, **185**, 23–33.

10 **Ovaert, T. C.** and **Pan J.** Optimal design of layered structures under normal (frictionless) contact loading. *Trans ASME J. Tribol.*, 2002, **124**, 438–442.

11 **Hooke, C. J.** The elastohydrodynamic lubrication of a cylinder on an elastic layer. *Wear*, 1986, **111**(1), 83–99.

12 **Elsharkawy, A. A.** and **Hamrock, B. J.** Elastohydrodynamic Lubrication of elastomeric-coated surfaces in line contact. *Proc. Instn Mech. Engrs, Part J: J. Engineering Tribology*, 1995, **209**, 119–130.

13 **Goryacheva, I., Sadeghi, F.,** and **Xu, C.** Viscoelastic effects in lubricated contacts. *Wear*, 1996, **198**, 307–312.

14 **Jaffar, M. J.** On the microelastohydrodynamic lubrication of an elastomeric bonded layer. *Tribol. Int.*, 2002, **35**, 193–200.

15 **Goglia, P. R., Cusano, C.,** and **Conry, T. F.** The effects of surface irregularities on the elastohydrodynamic lubrication of sliding line contacts, Part I–single irregularities; Part II–wavy surfaces. *Trans. ASME J. Tribol.*, 1984, **106**, 104–119.

16 **Lubrecht, A. A., Ten Napel, W. E.,** and **Bosma, R.** The influence of longitudinal and transverse roughness on the elastohydrodynamic lubrication of circular contacts. *Trans. ASME J. Tribol.*, 1988, **110**, 421–426.

17 **Kweh, C. C., Evans, H. P.,** and **Snidle, R. W.** Micro-elastohydrodynamic lubrication of an elliptical contact with transverse and three dimensional sinusoidal roughness. *Trans. ASME J. Tribol.*, 1989, **111**, 577–584.

18 **Elsharkawy, A. A.** and **Hamrock, B. J.** Subsurface stresses in micro-EHL line contacts. *Trans. ASME J. Tribol.*, 1991, **113**, 645–655.

19 **Chang, L., Webster, M. N.,** and **Jackson, A.** On the pressure rippling and roughness deformation in elastohydrodynamic lubrication of rough surfaces. *Trans. ASME J. Tribol.*, 1993, **115**, 439–444.

20 **Venner, C. H.** and **Lubrecht, A. A.** Transient analysis of surface features in an EHL line contact in the case of sliding. *Trans. ASME J. Tribol.*, 1994, **116**, 186–193.

21 **Hooke, C. J.** The effect of roughness in EHL contacts. Proceedings of 31st Leeds-Lyon Symposium on *Tribology*, 2005, pp. 31–46 (Elsevier, Amsterdam).

22 **Sadeghi, F.** A comparison of the fluid model's effect on the internal stresses of rough surfaces. *Trans. ASME J. Tribol.*, 1991, **113**, 142–149.

23 **Kweh, C. C., Patching, M. J., Evans, H. P.,** and **Snidle, R. W.** Simulation of elastohydrodynamic contacts between rough surfaces. *Trans. ASME J. Tribol.*, 1992, **114**, 412–419.

24 **Venner, C. H.** and **Ten Napel, W. E.** Surface roughness effects in an EHL line contact. *Trans. ASME J. Tribol.*, 1992, **114**, 186–191.

25 **Ai, X.** and **Cheng, H. S.** Transient EHL analysis for line contacts with measured surface roughness using multigrid technique. *Trans ASME J. Tribol.*, 1994, **116**, 549–558.

26 **Elcoate, C. D., Evans, H. P., Hughes, T. G.** and **Snidle, R. W.** Thin film, time dependent, micro-EHL solutions with real surface roughness. Proceedings of 25th Leeds–Lyon Symposium on *Tribology*, 1999, pp. 163–174, Elsevier, Amsterdam.

27 **Evans, H. P.** and **Snidle, R. W.** A model for elastohydrodynamic film failure in contacts between rough surfaces having transverse finish. *Trans. ASME J. Tribol.*, 1996, **118**(4), 847–857.

28 **Johnson, K. L.** and **Tevaarwark, J. L.** Shear behavior of elastohydro-dynamic oil films. *Proc. R. Soc. Lond. A*, 1977, **356**(12), 215–236.

29 **Hughes, T. G., Elcoate, C. D.,** and **Evans, H. P.** Coupled solution of the elastohydrodynamic line contact problem using a differential deflection method. *Proc. Instn Mech. Engrs, Part C: J. Mechanical Engineering Science*, 2000, **214**, 585–598.

30 **Elcoate, C. D., Evans, H. P., Hughes, T. G.,** and **Snidle, R. W.** Transient elastohydrodynamic analysis of rough surfaces using a novel coupled differential deflection method. *Proc. Instn Mech. Engrs, Part J: J. Engineering Tribology*, 2001, **215**, 319–337.

31 **Sneddon, I. N.** *Fourier transformation*, 1951 (McGraw Hill).

32 **Evans, H. P.** and **Hughes, T. G.** Evaluation of deflection in semi-infinite bodies by a differential method. *Proc. Instn Mech. Engrs. Part C: J. Mechanical Engineering Science*, 2000, **214**, 563–584.

33 **Evans, C. R.** and **Johnson, K. L.** The rheological properties of elastohydrodynamic lubricants. *Proc. Instn Mech. Engrs, Part C: J. Mechanical Engineering Science*, 1986, **200**, 303–312.

34 **Houpert, L.** and **Hamrock, B. J.** Elastohydrodynamic lubrication calculations as a tool to study scuffing. Proceedings of the 12th Leeds-Lyon Symposium on Tribology, 1985, pp. 146–155 (Mechanical Engineering Publications, Bury St. Edmunds, Suffolk, England).

35 **Conry, T. F., Wang, S.,** and **Cusano C.** A Reynolds-Eyring equation for elastohydrodynamic lubrication in line contacts. *Trans. ASME J. Tribol.*, 1987, **109**, 648–658.

36 **Ai, X.** and **Zeng, L.** A general model for micro-elastohydrodynamic lubrication and its full numerical solution. *Trans. ASME J. Tribol.*, 1989, **111**, 569–576.

37 **Jacod, B., Lugt, P. M., Dumont, M. L., Tripp, J. H.,** and **Venner, C. H.** Amplitude reduction of waviness in elastohydrodynamic lubrication using an eyring fluid model. *Proc. Instn Mech. Engrs, Part J: J. Engineering Tribology*, 2000, **214**, 343–350.

38 **Tao, G., Hughes, T. G., Evans, H. P., Snidle, R. W., Hopkinson, N. A., Talks, M.,** and **Starbuck, J. M.** Elastohydrodynamic lubrication analysis of gear tooth surfaces from micropitting tests *Trans. ASME J. Tribol.*, 2003, **125**, 267–274.

39 **Venner, C. H.** and **Lubrecht, A. A.** Numerical simulation of a transverse ridge in a circular EHL contact under rolling/sliding. *Trans. ASME J. Tribol.*, 1994, **116**, 751–761.

40 **Holmes, M. J. A., Qiao, H., Evans, H. P.,** and **Snidle, R. W.** Surface contact and damage in micro-EHL. Proceedings of 31st Leeds-Lyon Symposium on *Tribology*, 2005, pp. 605–616 (Elsevier, Amsterdam).

41 **Yoshida, A.** and **Fujii, M.** Influence of soft surface modification on rolling contact fatigue strength of machine elements. *Tribol. Int.*, 2002, **35**, 837–847.

APPENDIX

Notation

b	half-width of dry contact, (m)
b_{H}	Hertzian half-width of the contact for uncoated cylinders $[8w_zR/(\pi E')]^{1/2}$ (m)
E_{a}	modulus of elasticity of body a (Pa)
E_{b}	modulus of elasticity of body b (Pa)
E_{c}	modulus of elasticity of coating material (Pa)
E'	effective elastic modulus $2\left[\left(1-\nu_{\mathrm{a}}^2\right)/E_{\mathrm{a}}+\left(1-\nu_{\mathrm{b}}^2\right)/E_{\mathrm{b}}\right]^{-1}$, (Pa)
h	film thickness (m)
h_0	constant (m)
p	pressure (Pa)
p_{H}	maximum Hertzian pressure for uncoated cylinders, $[w_zE'/(2\pi R)]^{1/2}$ (Pa)
p_0	maximum contact pressure of dry contact (Pa)
R	effective radius of curvature, $R_{\mathrm{a}}R_{\mathrm{b}}/(R_{\mathrm{a}}+R_{\mathrm{b}})$ (m)
R_{a}	radius of body a (m)
R_{b}	radius of body b (m)
t_{c}	thickness of the coating layer (m)
u	velocity component in x-direction (m/s)
u_{a}	surface velocity of body a (m/s)
u_{b}	surface velocity of body b (m/s)
u_x	surface deflection in x-direction (m)
u_z	surface deflection in z-direction (m)
w_z	normal load per unit width (N/m)
x	coordinate direction tangential to surface (m)
x_{end}	outlet meniscus distance (m)
x_{min}	location of inlet pressure boundary (m)
z	vertical coordinate (m)
$\hat{z}$	pressure–viscosity index
α	pressure–viscosity coefficient
η	viscosity of the lubricant (Pa s)

η_0	viscosity of the lubricant at atmospheric pressure, (Pa s)	ρ_0	density of the lubricant at atmospheric pressure (kg/m^3)
ν_a	Poisson's ratio of body a	σ_x	normal stress in x-direction (Pa)
ν_b	Poisson's ratio of body b	σ_z	normal stress in z-direction (Pa)
ν_c	Poisson's ratio of coating material	τ_{xz}	shear stress perpendicular to x-direction and in z-direction (Pa)
ρ	density of the lubricant (kg/m^3)		